Article

Electronic Structure of the Peroxy Intermediate and Its Correlation to the Native Intermediate in the Multicopper Oxidases: Insights into the Reductive Cleavage of the O–O Bond

Jungjoo Yoon, and Edward I. Solomon

J. Am. Chem. Soc., **2007**, 129 (43), 13127-13136• DOI: 10.1021/ja073947a • Publication Date (Web): 05 October 2007

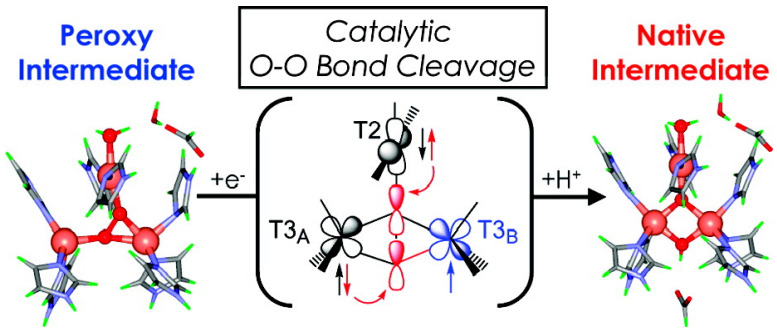

More About This Article

Additional resources and features associated with this article are available within the HTML version:

- Supporting Information
- Links to the 4 articles that cite this article, as of the time of this article download
- Access to high resolution figures
- Links to articles and content related to this article
- Copyright permission to reproduce figures and/or text from this article

View the Full Text HTML

J|A|C|S
ARTICLES
Published on Web 10/05/2007

Electronic Structure of the Peroxy Intermediate and Its Correlation to the Native Intermediate in the Multicopper Oxidases: Insights into the Reductive Cleavage of the O−O Bond

Jungjoo Yoon and Edward I. Solomon*

Contribution from the Department of Chemistry, Stanford University, Stanford, California 94305

Received May 31, 2007; E-mail: edward.solomon@stanford.edu

Abstract: The multicopper oxidases (MCOs) utilize a blue type 1 (T1) copper site and a trinuclear Cu cluster composed of a type 2 (T2) and a binuclear type 3 (T3) site that together catalyze the four-electron reduction of O_2 to H_2O. Reaction of the fully reduced enzyme with O_2 proceeds via two sequential two-electron steps generating the peroxy intermediate (PI) and the native intermediate (NI). While a detailed description of the geometric and electronic structure of NI has been developed, this has been more elusive for PI largely due to the diamagnetic nature of its ground state. Density functional theory (DFT) calculations have been used to correlate to spectroscopic data to generate a description of the geometric and electronic structure of PI. A highly conserved carboxylate residue near the T2 site is found to play a critical role in stabilizing the PI structure, which induces oxidation of the T2 and one T3 Cu center and strong superexchange stabilization via the peroxide bridge, allowing irreversible binding of O_2 at the trinuclear Cu site. Correlation of PI to NI is achieved using a two-dimensional potential energy surface generated to describe the catalytic two-electron reduction of the peroxide O−O bond by the MCOs. It is found that the reaction is thermodynamically driven by the relative stability of NI and the involvement of the simultaneous two-electron-transfer process. A low activation barrier (calculated ∼5−6 kcal/mol and experimental ∼3−5 kcal/mol) is produced by the triangular topology of the trinuclear Cu cluster site, as this symmetry provides good donor−acceptor frontier molecular orbital (FMO) overlap. Finally, the O−O bond cleavage in the trinuclear Cu cluster can be achieved via either a proton-assisted or a proton-unassisted process, allowing the MCOs to function over a wide range of pH. It is found that while the proton helps to stabilize the acceptor O_2^{2-} σ^* orbital in the proton-assisted process for better donor−acceptor FMO overlap, the third oxidized Cu center in the trinuclear site assumes the role as a Lewis acid in the proton-unassisted process for similarly efficient O−O bond cleavage.

1. Introduction

Multicopper oxidases (MCOs) are a family of enzymes that catalyze the four-electron reduction of O_2 to H_2O with concomitant oxidations of substrates.[1,2] To carry out their functions, all MCOs utilize the redox properties of four Cu centers. The electrons are taken up at the type 1 (T1) blue Cu site and transferred ∼13 Å to the trinuclear Cu cluster site composed of a type 2 (T2) normal Cu site and a type 3 (T3) coupled-binuclear copper site,[3,4] where the four-electron reduction of O_2 to H_2O occurs. In the fully oxidized resting form of the enzyme, each of the two T3 Cu centers is held in the protein by three His ligands and are bridged by a OH^- ligand, while the T2 is held by two His ligands and has an OH^- ligand outside the cluster (Figure 1).[5−15]

The catalytic cycle is initiated by the reaction of the fully reduced enzyme with O_2. In the fully reduced form, the T3 OH^- bridging ligand and T2 OH^- ligand are lost, leading to a coordinatively unsaturated trinuclear Cu cluster.[14,16,17] The reaction of the fully reduced enzyme with O_2 proceeds via two

(1) Solomon, E. I.; Chen, P.; Metz, M.; Lee, S. K.; Palmer, A. E. *Angew. Chem., Int. Ed.* **2001**, *40*, 4570−4590.
(2) Solomon, E. I.; Sundaram, U. M.; Machonkin, T. E. *Chem. Rev.* **1996**, *96*, 2563−2605.
(3) Cole, J. L.; Tan, G. O.; Yang, E. K.; Hodgson, K. O.; Solomon, E. I. *J. Am. Chem. Soc.* **1990**, *112*, 2243−2249.
(4) Spira-Solomon, D. J.; Allendorf, M. D.; Solomon, E. I. *J. Am. Chem. Soc.* **1986**, *108*, 5318−5328.
(5) Messerschmidt, A.; Ladenstein, R.; Huber, R.; Bolognesi, M.; Avigliano, L.; Petruzzelli, R.; Rossi, A.; Finazzi-Agró, A. *J. Mol. Biol.* **1992**, *224*, 179−205.
(6) Ducros, V.; Brzozowski, A. M.; Wilson, K. S.; Brown, S. H.; Østergaard, P.; Schneider, P.; Yaver, D. S.; Pedersen, A. H.; Davies, G. J. *Nat. Struct. Biol.* **1998**, *5*, 310−316.
(7) Zaitseva, I.; Zaitsev, V.; Card, G.; Moshkov, K.; Bax, B.; Ralph, A.; Lindley, P. *J. Biol. Inorg. Chem.* **1996**, *1*, 15−23.
(8) Bertrand, T.; Jolivalt, C.; Briozzo, P.; Caminade, E.; Joly, N.; Madzak, C.; Mougin, C. *Biochemistry* **2002**, *41*, 7325−7333.
(9) Piontek, K.; Antorini, M.; Choinowski, T. *J. Biol. Chem.* **2002**, *277*, 37663−37669.
(10) Hakulinen, N.; Kiiskinen, L. L.; Kruus, K.; Saloheimo, M.; Paananen, A.; Koivula, A.; Rouvinen, J. *Nat. Struct. Biol.* **2002**, *9*, 601−605.
(11) Roberts, S. A.; Weichsel, A.; Grass, G.; Thakali, K.; Hazzard, J. T.; Tollin, G.; Rensing, C.; Montfort, W. R. *Proc. Natl. Acad. Sci. U.S.A.* **2002**, *99*, 2766−2771.
(12) Enguita, F. J.; Marcal, D.; Martins, L. O.; Grenha, R.; Henriques, A. O.; Lindley, P. F.; Carrondo, M. A. *J. Biol. Chem.* **2004**, *279*, 23472−23476.
(13) Smith, A. W.; Camara-Artigas, A.; Wang, M. T.; Allen, J. P.; Francisco, W. A. *Biochemistry* **2006**, *45*, 4378−4387.
(14) Taylor, A. B.; Stoj, C. S.; Ziegler, L.; Kosman, D. J.; Hart, P. J. *Proc. Natl. Acad. Sci. U.S.A.* **2005**, *102*, 15459−15464.

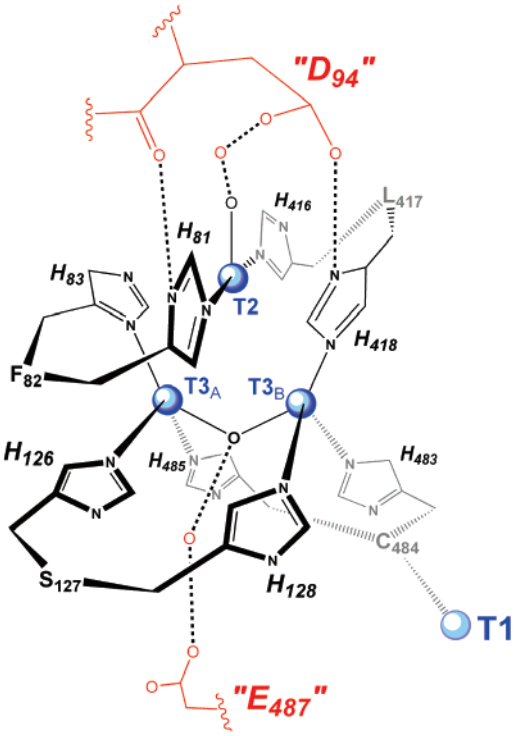

Figure 1. A general description of the trinuclear Cu cluster in multicopper oxidases. For the purpose of correlating to the earlier mutation studies on Fet3p, the residue numbers of Fet3p are given. Note that two nearby carboxylate residues in the second coordination sphere, D_{94} and E_{487}, are also indicated (in red). Mutant studies indicate that these residues have critical roles in the O_2 reactivity of the trinuclear Cu cluster.

sequential two-electron steps, generating the peroxy intermediate (PI) and the native intermediate (NI). In the holo-enzyme, only the four-electron reduced NI has been trapped[18−22] as the second two-electron process is very fast ($k > 350\ s^{-1}$),[23] effectively resulting in one four-electron process. Extensive spectroscopic studies on NI,[18] combined with model[24−28] and computational studies,[29] have demonstrated that NI is a fully oxidized species with O_2 fully reduced to water-level products that remain bound to the trinuclear site as μ_3-oxo and μ_2-hydroxo bridging ligands.

Alternatively, PI has been trapped and characterized using T1-depleted derivatives of MCOs, where the T1 is either replaced by a spectroscopic and redox-innocent Hg^{2+} ion in the case of laccase (T1HgLc)[23,30,31] or simply knocked out by mutating the Cys residue at the T1 site to Ser in Fet3p (T1D).[32−35] In the T1D forms, only three electrons are nominally available to reduce O_2, of which two from the three Cu centers in the trinuclear site are transferred to O_2. This leads to the formation of PI in a pH-independent and rapid process ($k \approx 2 \times 10^6\ M^{-1}\ s^{-1}$).[23,36] Alternatively, the decay of PI is very slow and pH dependent ($k \approx 0.003\ s^{-1}$ at pH = 4.7 and $k \approx 0.0003\ s^{-1}$ at pH 7.5 for T1HgLc, $pK_a \approx 5.7$).[23,34,35] It exhibits different kinetic behavior at different pH conditions, where an inverse proton kinetic isotope effect is observed at low pH ($k_H/k_D = 0.89$), while no such effect is observed at high pH ($k_H/k_D \approx 1$).[23,34,35,37] Importantly, it has been found by MCD spectroscopy that PI decays via an "NI-like" species.[31] This, along with the similar rate of formation of PI and NI, has indicated PI is a kinetically competent precursor to NI.[23,31]

The geometric and electronic structure of PI is less well defined than that of NI due the diamagnetic nature of its ground state ($S_{tot} = 0$, $-2J > 200\ cm^{-1}$).[31] Earlier studies have suggested that two electrons are donated by the two T3 Cu's in the trinuclear site to O_2 upon formation of PI in analogy to the O_2 reactivities in the other T3 sites in biology, hemocyanin (Hc) and tyrosinase (Tyr), where the oxy-forms acquire a μ-η^2:η^2 side-on-bridged geometric and electronic structure.[38−40] However, the spectral features of PI are very different from those of oxy-Hc and oxy-Tyr, indicating that the PI acquires a very different geometry.[31] It has been suggested that the peroxide must be bound internally in the trinuclear site as a T2−T3 bridging ligand,[23,31] which is supported by a spectroscopic study of the peroxy adduct (PA) of T1HgLc,[41] a crystallographic study of the PA of CotA,[17] and QM/MM calculations of PI and PA.[29]

In this study, extensive DFT calculations are correlated to spectroscopic data to develop the geometric and electronic structure of PI. This is then correlated to that of NI, which has been rigorously defined in previous studies,[24−28] to elucidate the reductive cleavage of the O−O bond (i.e., PI → NI). The roles of two highly conserved carboxylate residues (D_{94} and E_{487} in Fet3p, Figure 1) in the outer coordination sphere of the trinuclear cluster site are also evaluated and found to be essential in the stabilization of the PI structure and in proton donation in the O−O bond cleavage step. This study provides new molecular level insights into the role of the trinuclear Cu cluster site in the reaction mechanism of catalytic O_2 reduction in the MCOs.

(15) Garavaglia, S.; Cambria, M. T.; Miglio, M.; Ragusa, S.; Iacobazzi, V.; Palmieri, F.; D'Ambrosio, C.; Scaloni, A.; Rizzi, M. *J. Mol. Biol.* **2004**, *342*, 1519−1531.
(16) Messerschmidt, A.; Luecke, H.; Huber, R. *J. Mol. Biol.* **1993**, *230*, 997−1014.
(17) Bento, I.; Martins, L. O.; Lopes, G. G.; Carrondo, M. A.; Lindley, P. F. *Dalton Trans.* **2005**, 3507−3513.
(18) Lee, S. K.; George, S. D.; Antholine, W. E.; Hedman, B.; Hodgson, K. O.; Solomon, E. I. *J. Am. Chem. Soc.* **2002**, *124*, 6180−6193.
(19) Brändén, R.; Deinum, J. *Biochim. Biophys. Acta* **1978**, *524*, 297−304.
(20) Aasa, R.; Brändén, R.; Deinum, J.; Malmström, B. G.; Reinhammar, B.; Vänngård, T. *FEBS Lett.* **1976**, *61*, 115−119.
(21) Manabe, T.; Manabe, N.; Hiromi, K.; Hatano, H. *FEBS Lett.* **1972**, *23*, 268−270.
(22) Machonkin, T. E.; Solomon, E. I. *J. Am. Chem. Soc.* **2000**, *122*, 12547−12560.
(23) Palmer, A. E.; Lee, S. K.; Solomon, E. I. *J. Am. Chem. Soc.* **2001**, *123*, 6591−6599.
(24) Yoon, J.; Mirica, L. M.; Stack, T. D. P.; Solomon, E. I. *J. Am. Chem. Soc.* **2004**, *126*, 12586−12595.
(25) Yoon, J.; Mirica, L. M.; Stack, T. D. P.; Solomon, E. I. *J. Am. Chem. Soc.* **2005**, *127*, 13680−13693.
(26) Yoon, J.; Solomon, E. I. *Inorg. Chem.* **2005**, *44*, 8076−8086.
(27) Yoon, J.; Solomon, E. I. *Coord. Chem. Rev.* **2007**, *251*, 379−400.
(28) Yoon, J.; Liboiron, B. D.; Sarangi, R.; Hodgson, K. O.; Hedman, B.; Solomon, E. I. *Proc. Natl. Acad. Sci. U.S.A.* **2007**, *104*, 13609−13614.
(29) Rulíšek, L.; Solomon, E. I.; Ryde, U. *Inorg. Chem.* **2005**, *44*, 5612−5628.
(30) Morie-Bebel, M. M.; Morris, M. C.; Menzie, J. L.; McMillin, D. R. *J. Am. Chem. Soc.* **1984**, *106*, 3677−3678.
(31) Shin, W.; Sundaram, U. M.; Cole, J. L.; Zhang, H. H.; Hedman, B.; Hodgson, K. O.; Solomon, E. I. *J. Am. Chem. Soc.* **1996**, *118*, 3202−3215.
(32) Hassett, R. F.; Yuan, D. S.; Kosman, D. J. *J. Biol. Chem.* **1998**, *273*, 23274−23282.
(33) Blackburn, N. J.; Ralle, M.; Hassett, R.; Kosman, D. J. *Biochemistry* **2000**, *39*, 2316−2324.
(34) Palmer, A. E.; Quintanar, L.; Severance, S.; Wang, T. P.; Kosman, D. J.; Solomon, E. I. *Biochemistry* **2002**, *41*, 6438−6448.
(35) Quintanar, L.; Stoj, C.; Wang, T. P.; Kosman, D. J.; Solomon, E. I. *Biochemistry* **2005**, *44*, 6081−6091.
(36) Cole, J. L.; Ballou, D. P.; Solomon, E. I. *J. Am. Chem. Soc.* **1991**, *113*, 8544−8546.
(37) Augustine, A. J.; Quintanar, L.; Stoj, C. S.; Kosman, D. J.; Solomon, E. I. *J. Am. Chem. Soc.* **2007**, *129*, 13118−13126.
(38) Magnus, K. A.; Hazes, B.; Tonthat, H.; Bonaventura, C.; Bonaventura, J.; Hol, W. G. J. *Proteins* **1994**, *19*, 302−309.
(39) Matoba, Y.; Kumagai, T.; Yamamoto, A.; Yoshitsu, H.; Sugiyama, M. *J. Biol. Chem.* **2006**, *281*, 8981−8990.
(40) Cuff, M. E.; Miller, K. I.; van Holde, K. E.; Hendrickson, W. A. *J. Mol. Biol.* **1998**, *278*, 855−870.
(41) Sundaram, U. M.; Zhang, H. H.; Hedman, B.; Hodgson, K. O.; Solomon, E. I. *J. Am. Chem. Soc.* **1997**, *119*, 12525−12540.

2. Computational Details

DFT calculations were performed using Gaussian 03,[42] implementing the broken-symmetry method.[43] All geometry optimizations were performed using B3LYP functional[44] with double-ζ basis sets 6-31G* for Cu and coordinated N/O atoms and 3-21G* for the rest. The starting geometry of the trinuclear Cu site was adapted from the crystal structure of *Trametes versicolor* laccase (1GYC, Res. 1.9 Å),[9] where the His ligands were replaced by imidazolyl ligands. To reflect the features of the crystal structure, (a) the positions of the H atoms that replaced the side chains to the protein backbone and those bound to His N not bound to Cu (which are all involved in hydrogen bonds) were fixed, (b) the angle of the O atom on the T2 water-derived ligand relative to the plane of the two T2 His rings to prevent it from artificial binding to the nearby T3 His ligands was fixed, and (c) the three N-$T3_A$−$T3_B$-N dihedral angles ($T3_A$ and $T3_B$ are defined in Figure 1), where the N's are the coordinated atoms of the eclipsed His ligands, were fixed to keep the eclipsed conformation as found in the crystal structures of all MCOs. Note that the flexibility of the model was not affected by these constraints, as exemplified by the wide range of $T3_A$−$T3_B$ distances found in different structures (e.g., in PI, $R(T3_A-T3_B) = 4.07$ Å and in NI, $R(T3_A-T3_B) = 3.01$ Å). Additional details of the individual models are given in Results and Analysis. The resulting optimized structures of PI (with D_{94}), PI+e, PI+e+H, TS_1, TS_2, and NI (vide infra; the coordinates of these structures are given in Supporting Information) were further used for single-point calculations with the B3LYP functional using the triple-ζ basis set 6-311G* for Cu and coordinated N/O atoms and double-ζ 6-31G* for the rest. Solvation effects were also considered for PI+e, PI+eH, TS_1, TS_2, and NI (vide infra) using the polarized continuum model as implemented in Gaussian 03 (PCM/UAKS) with a dielectric constant of 4.0 to reflect the protein dielectric media. The molecular orbital (MO) compositions were obtained using PyMOlize.[45]

3. Results and Analysis

3.1. The Peroxy Intermediate. 3.1.1. Geometric Structure of PI. To obtain a spectroscopically relevant structure of PI, we have performed spin unrestricted DFT calculations, where O_2 is bound internally to the cluster as implicated by previous spectroscopic[41] and QM/MM computational results.[29,46] H_2O was chosen as the water-derived ligand on the T2 center, and the internal peroxide was kept unprotonated, following earlier kinetic data[23] indicating that the formation of PI is a pH-independent process.

Initially, model systems with only the ligands that are directly coordinated to the three Cu centers (the eight His and the T2 H_2O, Figure 1) were considered. All geometry optimizations were performed in the broken-symmetry $M_S = 0$ ($\langle S^2\rangle \approx 1.0$) states. Two structures were obtained, one with a side-on μ-η^2:η^2-O_2^{2-} geometry and the other with a μ_3-1,1,2-O_2^{2-} geometry (Figure 2 and Table 1; additional geometric parameters and spin densities are listed in Tables S1 and S2).[47] The former is reminiscent of oxy-Hc/Tyr,[1,2,48] while the latter is similar to that obtained in the QM/MM calculations of PI.[29,46] Both structures have singlet ground states, the side-on structure with $J \approx -3700$ cm^{-1} and the μ_3-1,1,2 structure with $J \approx -54$ cm^{-1},[49] reasonably consistent with experiment ($-2J > 200$ cm^{-1}).[31]

Of these two structures, the side-on structure was found to be energetically more stable by ~7.7 kcal/mol (pure singlet $S_{tot} = 0$ energy comparisons from projection of the broken-symmetry $M_S = 0$ energies).[49] However, this is inconsistent with experiment, as PI does not exhibit the spectral features of the side-on-bridged structure as found in oxy-Hc/Tyr and its model complexes, which are characterized by a prominent band in the absorption spectrum at ~340 nm with $\epsilon \approx 20000-25000$ M^{-1} cm^{-1} (see Figure S1).[1,2,48,50] In PI, while an absorption band at a similar energy is also observed, its intensity is 4−5 fold lower (vide infra), indicating that the side-on-bridged structure is not present in PI.[31]

Modified structures were then considered, implementing the possible effect of a nearby carboxylate residue, D_{94} (following

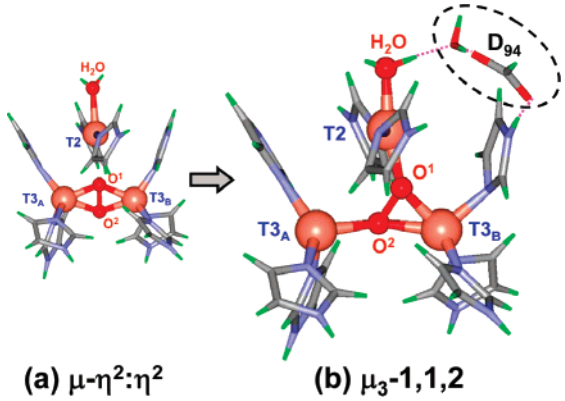

Figure 2. Calculated structures of PI, (a) without D_{94}, resulting in a side-on μ-η^2:η^2-bridged geometry, and (b) with D_{94}, resulting in a μ_3-1,1,2-bridged geometry. Refer to Table 1 for geometric parameters.

Table 1. Geometric Parameters for PI with and without D_{94} (distances in Å and angles in deg)[a]

	without D_{94} [μ-η^2:η^2]	with D_{94} [μ_3-1,1,2]	
O^1−O^2	1.475	1.457	(1.435)
T2−$T3_A$	3.801	4.007	(4.063)
T2−$T3_B$	4.006	3.682	(3.714)
$T3_A$−$T3_B$	3.686	4.066	(4.197)
T2−H_2O	2.390	1.997	(2.070)
T2−O^1	2.659	1.937	(1.973)
$T3_A$−O^1	2.012	3.098	(3.173)
$T3_A$−O^2	1.979	2.062	(2.199)
$T3_B$−O^1	2.032	1.937	(1.943)
$T3_B$−O^2	1.928	2.045	(2.033)
T2−O^1−$T3_B$	−	143.8	(143.0)
$T3_A$−O^1−$T3_B$	131.4	−	−
$T3_A$−O^2−$T3_B$	141.3	163.8	(165.3)

[a] Geometric parameters presented are those obtained using B3LYP functional with 6-31G* basis set on Cu and coordinated N/O atoms and 3-21G* on the rest. In addition, those obtained using B3LYP functional with 6-311G* basis set on Cu and coordinated N/O atoms and 6-31G* on the rest are indicated in parentheses for the μ_3-1,1,2-bridged structure.

(42) Frisch, M. J.; et al. *Gaussian 03*, revision C.01; Gaussian, Inc.: Pittsburgh, PA, 2004.
(43) Noodleman, L. *J. Chem. Phys.* **1981**, *74*, 5737−5743.
(44) Becke, A. D. *J. Chem. Phys.* **1993**, *98*, 5648−5652.
(45) Tenderholt, A. *PyMOlyze*, ver. 1.5; Stanford University: Stanford, CA, 2006.
(46) Chalupský, J.; Neese, F.; Solomon, E. I.; Ryde, U.; Rulíšek, L. *Inorg. Chem.* **2006**, *45*, 11051−11059.
(47) An additional geometry optimization on the μ_3-1,1,2-O_2^{2-}-bridged PI structure was performed with a larger basis set, with triple-ζ 6-311G* on Cu and coordinated N/O atoms and 6-31G* on the rest, to verify that the structures obtained in this study with the double-ζ quality basis set, with 6-31G* on Cu and coordinated N/O atoms and 3-21G* on the rest, are sound. As a result, it is found that the overall structure of PI remains the same and the geometric parameters are very similar to those obtained with the double-ζ basis set, as indicated in Table 1.
(48) Mirica, L. M.; Ottenwaelder, X.; Stack, T. D. P. *Chem. Rev.* **2004**, *104*, 1013−1045.
(49) These energies are based on calculations using B3LYP functional with 6-31G* basis set on Cu and coordinated N/O atoms and 3-21G* basis set on the rest.
(50) Eickman, N. C.; Himmelwright, R. S.; Solomon, E. I. *Proc. Natl. Acad. Sci. U.S.A.* **1979**, *76*, 2094−2098.

the residue numbering in Fet3p, Figure 1), which is highly conserved throughout all known MCOs.[5−15] X-ray crystal structures indicate that the carboxylate moiety of this residue is involved in hydrogen-bonding interactions with both the T2 water-derived ligand (mediated by a water molecule) and a $T3_B$ His ligand (Figure 1). In addition, the backbone carbonyl group of this residue is also hydrogen bonded to the δ-*N* of one of the T2 His ligands (Figure 1). In fact, the hydrogen-bonding connectivity of this residue has been observed to affect the T2 Cu^{II} site in the resting enzyme,[51] suggestive of a critical role in keeping the structural stability and in tuning the reactivity of the trinuclear cluster site. In addition, mutation of this residue to an uncharged residue, Ala or Asn, in Fet3p resulted in complete loss of O_2 reactivity.[35] Alternatively, the O_2 reactivity is completely retained in the $D_{94}E$ mutant of Fet3p, suggesting that the negative charge of D_{94} plays a significant role in the formation of PI.[35,37]

D_{94} was implemented in both the μ-η^2:η^2-O_2^{2-} side-on and μ_3-1,1,2-O_2^{2-} structures using a formate ion and a water molecule that mediate hydrogen-bonding interactions between D_{94} and the T2 water-derived ligand in the enzyme (Figure 2b). The H atom of the formate ion was fixed in position during the optimization, while other atoms of the formate ion and the water molecule were freely optimized. As a result, the μ_3-1,1,2-O_2^{2-} structure became more stable than the side-on structure by ~6.5 kcal/mol (pure singlet $S_{tot} = 0$ energy comparisons from projection of the broken-symmetry $M_S = 0$ energies).[49] The marked stabilization of the μ_3-1,1,2-O_2^{2-} structure derives from stronger T2− and $T3_B$−peroxide bonding interactions induced by the negative charge of D_{94} that lowers the reduction potentials of these Cu centers. In addition, the calculated *J* is −670 cm^{-1}, and it represents a highly stabilized singlet ground state via strong antiferromagnetic superexchange interactions. The μ_3-1,1,2-bridged geometry is also consistent with the EXAFS data, in which an intense outer-shell peak at ~3.4 Å is observed.[31] This EXAFS feature likely derives from the T2−$T3_B$ Cu pair (calculated distance = 3.68 Å, Table 1), as the strong T2− and $T3_B$−peroxide bonding interactions and the tight T2−O_2^{2-}−$T3_B$ bridge would promote the favorable Debye−Waller factor required for the intense outer-shell peak ($T3_A$ and $T3_B$ are defined in Figure 2).

3.1.2. Electronic Structure of PI: Correlation to Spectroscopy. Due to the lack of EPR and MCD features, specific assignments of the oxidation states of the three Cu centers in PI have been difficult. While it has been previously proposed that the two T3 Cu's in PI are oxidized as in Hc/Tyr, the distinct nature of the T3 sites in MCOs relative to Hc/Tyr has been demonstrated with the T2-depleted derivative of Lc which lacks any affinity toward O_2.[52−54]

In the calculated μ_3-1,1,2-bridged PI structure with D_{94} (Figure 2b), it is found that the T2 and $T3_B$ are oxidized and $T3_A$ is reduced. This description of the oxidiation states of the Cu centers in PI is consistent with the available spectroscopic data on PI and its structural analogue, the peroxy adduct (PA).[41] In PA, which is obtained by binding H_2O_2 to the fully oxidized trinuclear Cu cluster in T1HgLc, all three Cu centers are oxidized with a paramagnetic $S_{tot} = {}^1/_2$ ground state, rendering it to be EPR and MCD active. Importantly, it has been established that the peroxide binding geometries in PA and PI are similar (e.g., both show the characteristic intense outer-shell peak in the EXAFS Fourier transform data at ~3.4 Å), demonstrating PA to be a valid structural analogue of PI.[41]

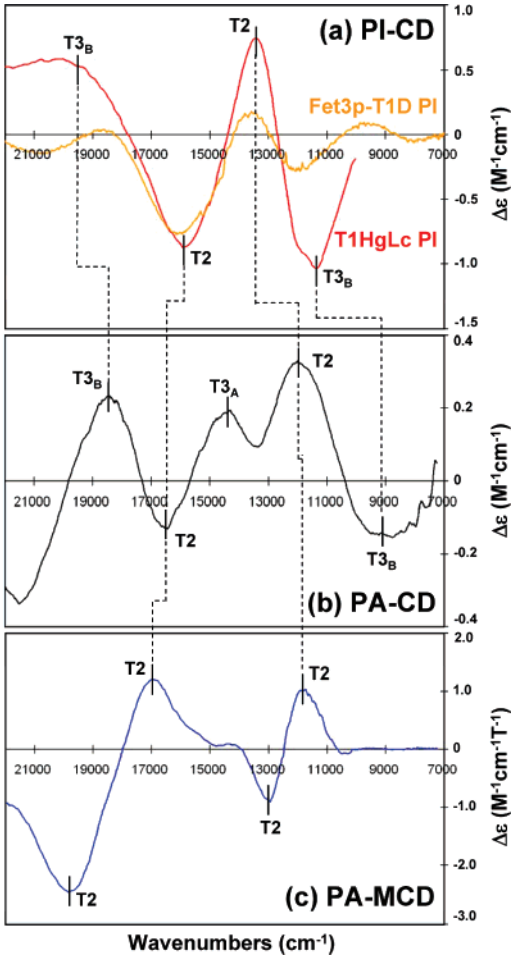

Figure 3. Comparison and assignments of the LF transitions in PI and PA of T1HgLc in the CD and MCD spectra, adapted from earlier studies (refs 31 and 41). (a) 298 K CD spectrum of PI, where PI of T1HgLc is given in red (100 mM potassium phosphate buffer, pH = 7.4). 298 K CD spectrum of PI from Fet3p-T1D is also given in orange (100 mM sodium phosphate buffer, pH = 7.4) to show CD features below 10000 cm^{-1} (adapted from ref 37). (b) 298 K CD spectrum of PA (T1HgLc + 200-fold excess of H_2O_2, 100 mM potassium phosphate buffer, pH = 6.0). (c) 4.2 K MCD spectrum of PA (T1HgLc + 200-fold excess of H_2O_2, 100 mM potassium phosphate buffer, pH = 6.0). Indicated peak positions are based on simultaneous Gaussian fitting results using absorption, CD (for PI and PA), and MCD spectra (for PA).

In Figure 3, the 298K CD spectra of PI and PA and 4.2 K MCD spectrum of PA in the ligand field region are presented, where band positions are indicated on the basis of previous simultaneous Gaussian fitting results using absorption, CD, and MCD (for PA) spectra.[31,41] Four bands are observed in the PA MCD spectrum that are all associated with the paramagnetic T2 Cu^{II} center, the $S = {}^1/_2$ spin being localized at the T2 Cu^{II} center in PA as previously determined by the EPR data.[41] Alternatively, at least five bands are observed in the PA CD spectrum. Previously, these CD bands were assigned to the T3

(51) Quintanar, L.; Yoon, J.; Aznar, C. P.; Palmer, A. E.; Andersson, K. K.; Britt, R. D.; Solomon, E. I. *J. Am. Chem. Soc.* **2005**, *127*, 13832−13845.
(52) Lubien, C. D.; Winkler, M. E.; Thamann, T. J.; Scott, R. A.; Co, M. S.; Hodgson, K. O.; Solomon, E. I. *J. Am. Chem. Soc.* **1981**, *103*, 7014−7016.
(53) Penner-Hahn, J. E.; Hedman, B.; Hodgson, K. O.; Spira, D. J.; Solomon, E. I. *Biochem. Biophys. Res. Commun.* **1984**, *119*, 567−574.
(54) Spira-Solomon, D. J.; Solomon, E. I. *J. Am. Chem. Soc.* **1987**, *109*, 6421−6432.

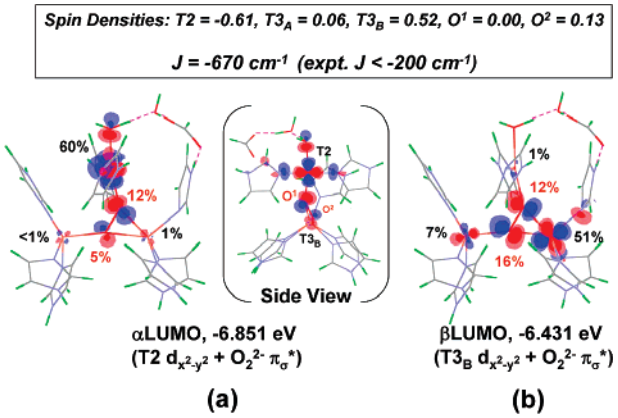

Figure 4. Contours of the α- and *β*-LUMOs of PI+D_{94} that are based on T2 $d_{x^2-y^2}$ and $T3_B$ $d_{x^2-y^2}$, respectively, obtained from the broken-symmetry state ($M_S = 0$) calculation. Both LUMOs have significant peroxide π_σ* characters. Overall spin densities, isotropic exchange constant *J*, and the % compositions are indicated, Cu centers in black and O atoms of peroxide in red. The side view of α-LUMO is also shown in (a) for better view of the T2 $d_{x^2-y^2}$ orbital.

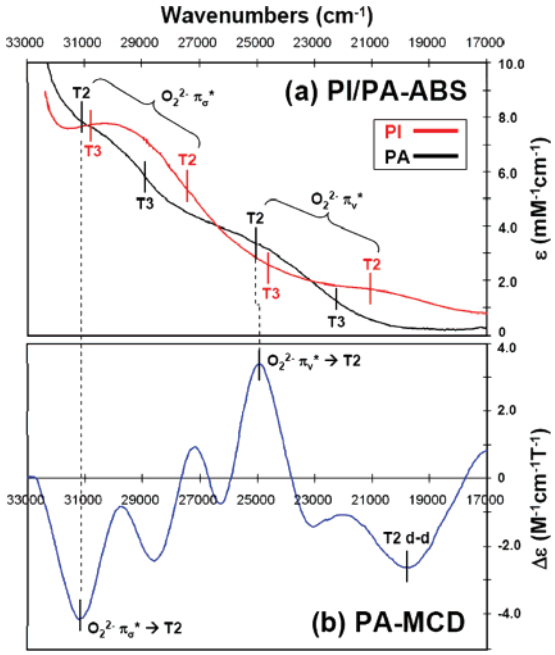

Figure 5. Comparison and assignments of the CT transitions in PI and PA of T1HgLc in the absorption and MCD spectra, adapted from earlier studies (refs 31 and 41). (a) 298 K absorption spectra of PI (red, 100 mM potassium phosphate buffer, pH = 7.4) and PA (black, T1HgLc + 200-fold excess of H_2O_2, 100 mM potassium phosphate buffer, pH = 6.0). (b) 4.2 K MCD spectrum of PA (T1HgLc + 200-fold excess of H_2O_2, 100 mM potassium phosphate buffer, pH = 6.0). Indicated peak positions are based on simultaneous Gaussian fitting results using absorption, CD (for PI and PA), and MCD spectra (for PA). Note that bands not assigned in the MCD spectrum are associated with His → T2 CT transitions.

Cu's by analogy to the resting oxidized enzyme where only the T3 Cu's contribute to the CD spectrum. However, it is now established that the structure of PA is significantly different from that of the resting oxidized enzyme (Figure 1) as the T3 OH^- bridge of the resting enzyme is replaced by the peroxide in PA (and PI, Figure 2b). Thus, it is possible that both the T2 and T3 Cu's contribute to the CD spectrum of PA. In fact, two bands are found in both the CD and MCD spectra of PA at ~12000 cm^{-1} and ~17000 cm^{-1}, respectively (Figure 3b,c), indicating that these are associated with the T2 Cu site.

Comparing the CD spectra of PI and PA, four bands can be correlated to one another by their signs, energies, and intensities; the shifts in energies would derive from the differences in the electronic distributions in PI and PA. Importantly, the two PA CD bands associated with the T2 center, (+)12000 cm^{-1} and (−)17000 cm^{-1}, can be correlated to the PI CD bands at (+)-13300 cm^{-1} and (−)15900 cm^{-1}, respectively. The other PI CD bands, each of which correlates to a PA CD band, would then be associated with the other oxidized Cu center in PI (i.e., $T3_B$). Notably, there is a PA CD band at ~(+)14500 cm^{-1} that does not correlate to any band in the PI CD and PA MCD spectra. This band would be associated with the $T3_A$ center, which is reduced in PI (Figure 2b) and MCD-silent in PA.

With the validation that the description of the metal oxidation states in PI is consistent with experiment (with T2 and $T3_B$ oxidized and $T3_A$ reduced), the diamagnetic $S_{tot} = 0$ ground state can now be correlated to the calculated electronic structure of PI. As mentioned above, the isotropic exchange coupling constant, *J*, is calculated to be −670 cm^{-1}, indicative of a strong antiferromagnetic coupling between the spins at the two magnetic centers now considered to be the oxidized T2 and $T3_B$ centers that are bridged by the peroxide. Figure 4 presents the contours of the α- and *β*-LUMOs that are based on T2 Cu $d_{x^2-y^2}$ and $T3_B$ Cu $d_{x^2-y^2}$, respectively, which represent the two magnetic orbitals involved in the superexchange interaction in PI (Figure 2b). Both of these magnetic orbitals contain a significant amount of O_2^{2-} π_σ* character. As shown in Figure 4, the O_2^{2-} π_σ* orbital is involved in an asymmetric orbital interaction with the T2 and $T3_B$ Cu centers, in which the O_2^{2-} π_σ* orbital forms one *σ*-bond with the T2 Cu $d_{x^2-y^2}$ orbital in the T2-based magnetic orbital (Figure 4a), while it forms two *σ*-bonds with the $T3_B$ Cu $d_{x^2-y^2}$ orbital in the $T3_B$-based magnetic orbital (Figure 4b).[55] Importantly, the O_2^{2-} π_s* character allows good orbital overlap between T2- and $T3_B$-based magnetic orbitals at the bridging peroxide, which leads to the strong antiferromagnetic coupling in PI.

The calculated electronic structure of PI can also be correlated to the spectral features in the charge transfer (CT) region of the absorption spectrum of PI. In Figure 5a, the absorption spectrum of PI of T1HgLc is presented in red, where positions of the four CT bands associated with $O_2^{2-} \rightarrow Cu^{II}$ CT transitions are indicated on the basis of previous studies of PI in both the T1HgLc and T1D Fet3p.[31,34] The four bands can be categorized into the higher-energy/higher-intensity O_2^{2-} π_σ* → Cu^{II} (~31000 cm^{-1} and ~27500 cm^{-1}) and lower-energy/lower-intensity O_2^{2-} π_v* → Cu^{II} CT transitions (~25000 cm^{-1} and ~21000 cm^{-1}). Further distinction between the two O_2^{2-} π_σ* → Cu^{II} CT transitions can be made using the MO description of PI in Figure 4. The T2-based α-LUMO and $T3_B$-based *β*-LUMO, both of which are significantly mixed with the O_2^{2-} π_σ* orbital, would be good acceptor MOs for the O_2^{2-} π_σ* → Cu^{II} CT transitions, the donor MO being the doubly occupied MO based on O_2^{2-} π_σ*. The MO energies and O_2^{2-} π_σ* characters in these LUMOs can be directly correlated to the relative energies and intensities of the O_2^{2-} π_σ* → Cu^{II} CT transitions. As shown in Figure 4, the $T3_B$-based *β*-LUMO is higher in energy than the T2-based

(55) Note that the Cu−peroxide interactions found in PI are different from those of the μ-η^2:η^2-O_2^{2-} side-on-bridged structure where each of the Cu $d_{x^2-y^2}$ orbitals form two strong *σ*-bonds with the O_2^{2-} π_σ* orbital. As a result, the exchange coupling is larger in the side-on structure ($J \approx -3700$ cm^{-1},[49] vide supra) compared to that of PI ($J \approx -670$ cm^{-1}).

α-LUMO by 0.42 eV (~3400 cm^{-1}), and the peroxide character is higher by ~11% (the difference of the % character of both peroxide O atoms). On the basis of these descriptions, the higher-energy band at ~31000 cm^{-1} can be assigned to the O_2^{2-} $\pi_\sigma^* \rightarrow T3_B$ CT transition, and the lower-energy band at ~27500 cm^{-1}, to the O_2^{2-} $\pi_\sigma^* \rightarrow$ T2 CT transition.[56] Similar assignments can be applied to the other lower-energy CT bands, the O_2^{2-} $\pi_v^* \rightarrow T3_B$ and T2 CT transitions, as indicated in Figure 5a (red).

To further validate the above CT assignments in PI, the CT spectral features of PI are compared to those of PA. In Figure 5, the 298 K absorption (in black) and 4.2 K MCD spectra of PA are presented with band positions from a previous study.[41] As mentioned above, the features of the PA MCD spectrum are only associated with its paramagnetic T2 site. In the PA MCD spectrum, a definitive assignment was previously made for the intense (+) 25500 cm^{-1} band as a $O_2^{2-} \rightarrow$ T2 CT transition based on comparative analysis of absorption, CD, and MCD spectra.[41] From pulsed EPR data, the T2 water-derived ligand is OH^- in PA.[57] Due to the differences in ligand field, the T2-based acceptor MO in PA would be several thousand cm^{-1} higher than that of PI with H_2O as its T2 water-derived ligand. Indeed, the O_2^{2-} $\pi_v^* \rightarrow$ T2 CT transition in PI (Figure 5a (red), at ~21000 cm^{-1}) is found ~4000 cm^{-1} lower in energy than the 25500 cm^{-1} band in PA. Similarly, it is expected that the O_2^{2-} $\pi_\sigma^* \rightarrow$ T2 CT transition in PA is higher in energy by ~4000 cm^{-1} than that of PI observed at ~27500 cm^{-1}. The ~31000 cm^{-1} band in PA can thus be assigned as the O_2^{2-} $\pi_\sigma^* \rightarrow$ T2 CT transition, which is supported by the fact that it is observed in both the absorption and MCD spectra of PA.

3.2. O−O Bond Cleavage. With an experimentally calibrated description of the geometric and electronic structure of PI, we now extend our investigation toward correlating PI with NI to describe the O−O bond-cleavage reaction by the trinuclear Cu cluster in the MCOs. As mentioned in the Introduction, experiment indicates that PI is a kinetically competent precursor of the four-electron O_2-reduced NI and that the PI → NI process is the second two-electron step in the reaction mechanism that involves the O−O bond cleavage. This step is very fast in the native enzyme (k > 350 s^{-1}),[23,36] where an extra electron from T1 promotes the two-electron peroxide O−O bond cleavage. Notably, it also occurs during the decay of PI, which is slow (k ≈ 0.0003−0.003 s^{-1}) due to the lack of the T1 site as the nominal source of the fourth electron.

Thus, we model our starting geometry for O−O cleavage to NI with the PI structure obtained above (Figure 2b). In addition to the formate ion that mimics D_{94}, a formic acid is included to mimic the role of a second nearby carboxylate residue, E_{487} (Figure 1). From a recent Fet3p mutant study, E_{487} has been demonstrated to play a central role in proton donation in the decay of PI.[37] Moreover, the proton from E_{487} is necessary to form the OH^- bridge in NI. For the simplicity of the model, the position of the formic acid is moved closer to the T3 site than in the enzyme structure. In the crystal structures of resting MCOs, E_{487} (or the equivalent Asp/Glu) is hydrogen bonded to the T3 OH^- bridging ligand through one or two water molecules. Here, the mediating water is removed, and the formic acid is placed such that the O atom of the formic acid involved in the hydrogen bonding (designated O′, see Figure 6, inset) is at the position of the O atom of the removed water molecule. In addition, unless otherwise mentioned, the distance between the peroxide O atom (designated O^2, see Figure 6, inset) and the formic acid O′ atom is fixed at a value of 2.87 Å, which is a reasonable distance for the hydrogen bond (2.87 Å is the distance between the O atoms of T3 OH^- bridging ligand and the mediating water molecule in the crystal structure of resting *T. versicolor* laccase, from which the starting geometries for all of the calculations of this study have been obtained).[58]

3.2.1. PI with an Extra Electron from T1: PI+e. At the starting point of O−O bond cleavage, the extra electron from the T1 site is assumed to have been transferred to the PI structure, while the proton on the formic acid (designated H′, see Figure 6, inset) is not transferred. The resulting structure, designated PI+e, is shown in Figure 6. Notably, the structure of PI+e is considerably different from that of PI (Figure 2b). This structure derives from the occupation of the extra electron in the hole on the T2 center in PI (i.e., occupation of the α-LUMO in Figure 4), which is found to be lower in MO energy than the hole on the $T3_B$ center in PI (the β-LUMO in Figure 4). Due to the reduction of the T2 center, the T2−peroxide bonding interaction is lost, and consequently, PI+e acquires a structure with the peroxide in between $T3_B$ and $T3_A$ centers. The $T3_A$−peroxide bonding interaction, however, is found to be very limited as the $T3_A$ is also reduced, which is indicated by the low spin density on the $T3_A$ center (spin densities are T2 = 0.00, $T3_A$ = +0.07, $T3_B$ = +0.48 in PI+e).

3.2.2. Proton-Unassisted O−O Bond Cleavage. The energy changes along the peroxide O^1−O^2 bond elongation (see the inset of Figure 6 for atom designations) without proton transfer from the formic acid are investigated first. In addition to PI+e with $R(O^1-O^2)$ = 1.46 Å, partially optimized PI+e structures with fixed $R(O^1-O^2)$ = 1.50, 1.60, 1.70, 1.80, and 1.90 Å are obtained. At $R(O^1-O^2)$ > 1.90 Å, the proton transfer from the formic acid to the O^2 atom occurs spontaneously due to the increased negative charge on the O^2 center. Finally, the NI structure with O^2 protonated (i.e., the T3 OH^- bridge in NI) is obtained at $R(O^1-O^2)$ ≈ 2.40 Å. All optimizations are performed at the broken-symmetry states as the spin expectation value, $\langle S^2 \rangle$, deviates from the pure spin doublet value of $\langle S^2 \rangle \approx 0.75$ upon O−O bond elongation and spin redistribution among the Cu and peroxide O atoms. Two broken-symmetry spin configurations allow description of transient states along the O−O bond elongation as two electrons of opposite spins (↑ and ↓) are donated from the reduced T2 and $T3_A$ centers to the O_2^{2-} σ^* orbital in PI+e, $|T2T3_AT3_B\rangle = |\beta\alpha\alpha\rangle$ and $|\alpha\beta\alpha\rangle$. Of these, however, it is found that only the $|\beta\alpha\alpha\rangle$ spin configuration generates transient-state structures that describe continuous

(56) Resonance Raman experiments were performed on PI obtained from both T1Hg laccase and T1D Fet3p. However, we were not able to observe any vibrational signals above noise as these were dominated by the intense fluorescence of the aromatic residues when PI was irradiated in the near UV. Note that in oxy-hemocyanin, the intense absorption ($\epsilon \approx 20000$ M^{-1} cm^{-1}) quenches the fluorescence in this region, allowing the resonance Raman spectrum to be obtained.

(57) Unpublished results.

(58) To compare the energy difference between the direct proton transfer from a proton donor to a proton acceptor and the indirect proton transfer via a water molecule, we have modeled the proton-transfer process between a formate ion and a formic acid at the B3LYP/6-31++G** level. As a result, energy barriers for the proton-transfer process directly between a formate and a formic acid and that mediated by a water molecule were estimated with relatively similar values of ~7.9 and ~12.0 kcal/mol, respectively. (The distance between O atoms accepting and donating the proton was fixed at 2.80 Å. See Figures S2, S3 and figure legends for details of the calculations.)

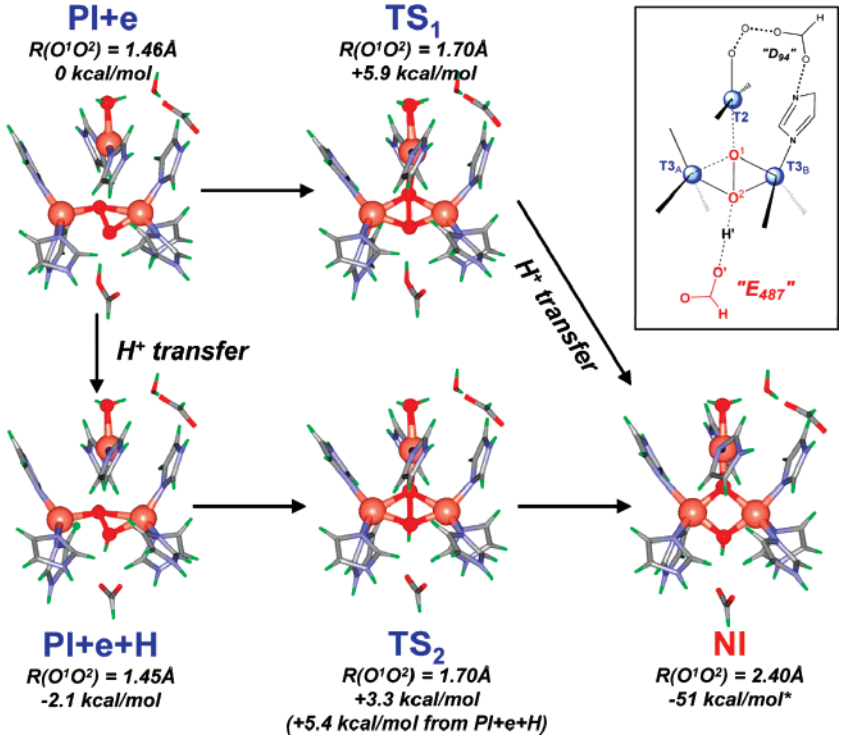

Figure 6. Calculated structures of PI+e, PI+e+H, TS_1, TS_2, and NI, where the two transition states, TS_1 and TS_2, refer to transition states in the proton-unassisted and proton-assisted O−O bond cleavage, respectively. (Inset) Designations of atoms are indicated. The energies are based on single-point calculations using B3LYP functional with 6-311G* for Cu and coordinated N/O atoms and 6-31G* for the rest, with additional consideration of solvation effects using the polarized continuum model (PCM/UAKS) with dielectric constant (ϵ) of 4.0. The geometry optimizations were performed using B3LYP functional with 6-31G* for Cu and coordinated N/O atoms and 3-21G* for the rest.

structural transition between PI+e and NI. In the $|\beta\alpha\alpha\rangle$ spin configuration, the same spin orientation on the two T3 Cu centers allows favorable electron delocalization over the T3 centers via the bridging O^1 and O^2 atoms. As a result, the O^1 and O^2 atoms remain bound to both the $T3_A$ and $T3_B$ centers (O^1 also bound to T2), and the O−O bond elongation occurs along the direction perpendicular to $T3_A$−$T3_B$ in the Cu_3 plane, leading to the NI structure with μ_3-oxo and T3 μ-OH^- bridging ligands. The O−O bond elongation in the $|\alpha\beta\alpha\rangle$ spin configuration, on the other hand, occurs along the direction perpendicular to T2−$T3_B$ in the Cu_3 plane, as the electron delocalization over the T2 and $T3_B$ centers via the O^1 atom results in the formation of a strong T2−O−$T3_B$ bridge with a wide bridging angle >150°. This leads to the dissociation of the O^1 atom from the $T3_A$ center, and consequently, the structures obtained with long $R(O^1-O^2)$ (>1.8 Å) do not correlate with the all-bridged structure of NI.[59]

The overall PI+e → NI process is highly exothermic, with $\Delta E = -51$ kcal/mol (obtained from comparison of the pure spin doublet energies of PI+e and NI, where the doublet energy of NI was obtained from projection of the energy of the broken-symmetry state $|T2T3_AT3_B\rangle = |\beta\alpha\alpha\rangle$ with $\langle S^2\rangle \approx 1.75$), indicating that this is a highly thermodynamically driven process. The transition state is located at $R(O^1-O^2) \approx 1.70$ Å (TS_1, Figure 6, top), with an activation energy estimated at +5.9 kcal/mol relative to PI+e. The low activation energy from these calculations is consistent with the experimental value of ∼3−5 kcal/mol, which is obtained from the experimental rate of $k >$ 350 s^{-1} for O−O bond cleavage, using the Arrhenius equation $k = A\exp(-E_a/RT)$, where the pre-exponential factor A is assumed to be in the order of 10^5−10^6. Importantly, this result implies that a proton is not required to drive the catalytic O−O bond-cleavage reaction in the MCOs, although it is required at a later stage (after TS_1) to protonate the T3 μ-oxo ligand, which otherwise would be energetically unfavorable.

3.2.3. Proton-Assisted O−O Bond Cleavage. Alternatively, the effect of protonation on the O−O bond-cleavage reaction is investigated by transferring the H′ atom on the formic acid to the peroxide O^2 atom. First, we investigate the structure of PI+e after the complete proton transfer was obtained (PI+e+H, Figure 6, bottom). The overall geometry of PI+e+H is very similar to that of PI+e, although it is found to be at lower energy than PI+e by ∼−2.1 kcal/mol. From this energy difference (neglecting entropy contributions), the pK_a of PI+e can be estimated to be ∼1.5 pH units higher than that of the proton donor (i.e., the formic acid in our model) at room temperature. Note also that the proton transfer in the PI+e → PI+e+H process is likely a kinetically unhindered process. With the fixed $R(O^2-O') = 2.87$ Å, it is estimated that the energy barrier for the proton transfer is ∼7.7 kcal/mol[49] (at $R(O^2-H') = 1.50$ Å, $R(O^1-O^2) = 1.46$ Å (fixed)). However, this activation energy is found to decrease with shorter $R(O^2-O')$. At $R(O^2-O') =$ 2.75 Å (fixed), the estimated activation energy is lowered to ∼3.9 kcal/mol (at $R(O^2-H') = 1.40$ Å and $R(O^1-O^2) = 1.46$ Å (fixed); Table S4), while at $R(O^2-O') = 2.60$ Å (fixed), no energy barrier is found (i.e., optimization of PI+e resulted in PI+e+H). Therefore, the activation barrier for the proton

(59) Note that three possible broken-symmetry states, with $|\beta\alpha\alpha\rangle$, $|\alpha\beta\alpha\rangle$, and $|\alpha\alpha\beta\rangle$ spin configurations, have very similar energies and contribute equivalently to the spin-frustrated ground state of NI.[28] Thus, while the $|\beta\alpha\alpha\rangle$ spin configuration contributes significantly in the early stage of O−O bond cleavage (which includes the transition state, vide infra), the other two spin configurations become equally important as all three Cu centers in the trinuclear cluster become oxidized.

transfer is largely dependent on the heavy atom distances, and in the flexible protein environment, the O atom distances would be dynamically optimized to accommodate the lower activation barrier for proton transfer to convert PI+e to the thermodynamically more stable PI+e+H form. This would be consistent with the enzyme where the proton transfer would be mediated by a water molecule between E_{487} and the peroxide.

The energy changes along the O^1-O^2 bond elongation in the PI+e+H structure are then investigated. In addition to PI+e+H with $R(O^1-O^2) = 1.45$ Å, partial optimizations of PI+e+H are performed at fixed $R(O^1-O^2)$ of 1.50, 1.60, 1.70, 1.80, 1.90, and 2.10 Å (plus NI with $R(O^1-O^2) \approx 2.40$ Å). As with PI+e, the broken-symmetry spin configuration of $|T2T3_AT3_B\rangle = |\beta\alpha\alpha\rangle$ is implemented in these calculations (vide supra). Assuming that the activation barrier of the proton transfer (PI+e → PI+e+H) is low,[60] the transition state for the PI+e → PI+e+H → NI process is located at $R(O^1-O^2) \approx 1.70$ Å (TS_2, Figure 6, bottom), where the activation energy is estimated +3.3 kcal/mol relative to PI+e and +5.4 kcal/mol relative to PI+e+H. As with PI+e, the low-energy barrier for this process is consistent with the experimental value of ~3−5 kcal/mol. Although not by much, the activation energy is smaller than that of the proton-unassisted PI+e → NI process, indicating that the proton does play a role in the cleavage of the O−O bond.

3.2.4. 2D-Potential Energy Surface: Two Possible Reaction Pathways. The proton-unassisted PI+e → NI and proton-assisted PI+e → PI+e+H → NI processes can be combined into a two-dimensional potential energy surface (2D-PES), which simultaneously accounts for the $R(O^1-O^2)$ and $R(O^2-H')$ reaction coordinates. The surface is generated using 28 points at different $R(O^1-O^2)$ and $R(O^2-H')$: at $R(O^1-O^2) =$ 1.46, 1.50, 1.60, 1.70 Å (i.e., up to TS_1 and TS_2), $R(O^2-H') =$ ~1.85, 1.70, 1.50, 1.30, ~1.0 Å; at $R(O^1-O^2) = 1.80$ and 1.90 Å, $R(O^2-H') =$ ~1.8, 1.50, ~1.0 Å; at $R(O^1-O^2) = 2.10$ and 2.40 Å, $R(O^2-H') =$ ~1.0 Å. The results are given in Table S3.

Starting from the rear diagonal in Figure 7, which is PI+e, and proceeding to the front diagonal, which is NI, two possible lowest-energy paths can be traced on the 2D-PES that are consistent with the proton-unassisted process (path 1: PI+e → TS_1 → NI) and the proton-assisted process (path 2 : PI+e → PI+e+H → TS_2 → NI). Recall that previous kinetic studies on PI decay in T1HgLc[23] and T1D Fet3p[34,35,37] have shown that an inverse proton kinetic isotope effect ($k_H/k_D = 0.89$) is involved at low pH (pH ≈ 5), whereas no isotope effect is present ($k_H/k_D \approx 1$) at high pH (pH ≈ 7). These kinetic isotope data suggest that the O−H bond from protonation of the peroxide must be present at the transition state at low pH and is not formed at the transition state at high pH.[37] Thus, the distinct kinetic descriptions of PI decay at different pH's can be directly correlated to paths 1 and 2 in the 2D-PES presented in Figure 7. In addition, the similarity in the activation energies of the proton-unassisted and proton-assisted processes of paths 1 and 2 (5.7 kcal/mol vs 5.4 kcal/mol) is also consistent with the similarity in the experimental activation energy of PI decay at high and low pH's, which only differ by ~1 kcal/mol.[23]

(60) As indicated in footnote 58, the energy barrier in the proton-transfer process is estimated to be higher when it is mediated by a water molecule. However, the relative stability of PI+e+H, compared to that of PI+e, can provide enough thermodynamic driving force to make the energy barrier in the proton-transfer process still small relative to the overall transition-state energy.

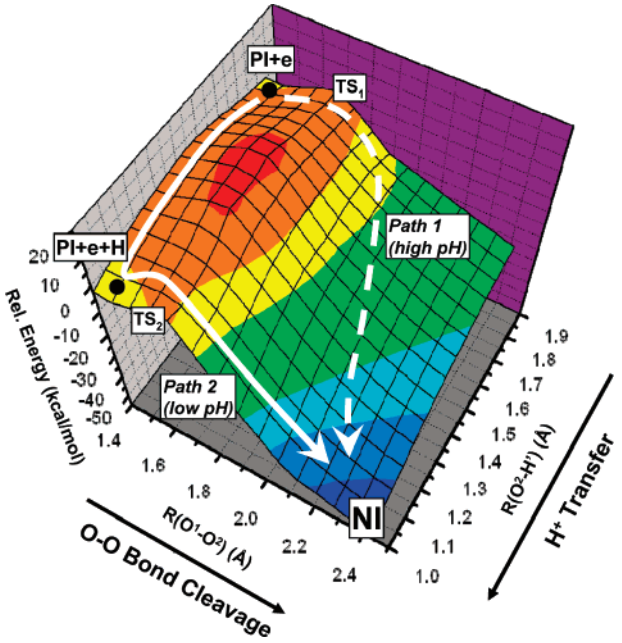

Figure 7. Two-dimensional potential energy surface (2D-PES) of the O−O bond cleavage in the multicopper oxidases. Refer to Figure 6, inset, for designation of O^1, O^2, and H′. The energies are based on calculations using B3LYP functional with 6-31G* for Cu and coordinated N/O atoms and 3-21G* for the rest.

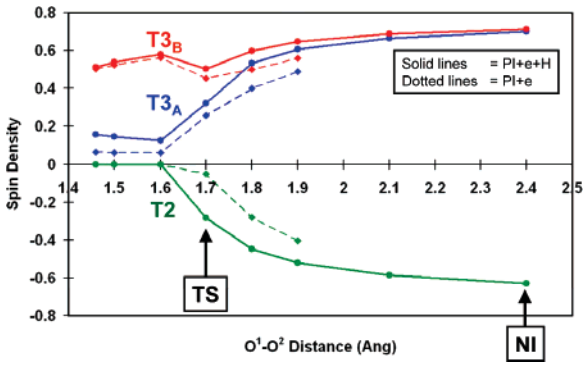

Figure 8. Changes in spin densities upon O−O bond elongation. Solid lines indicate changes from PI+e+H to NI (i.e., with protonated peroxide), and dotted lines indicate changes from PI+e. PI+e with $R(O^1-O^2) > 1.9$ Å are not shown, as the proton transfer occurs spontaneously with no barrier at these O^1-O^2 distances.

3.2.5. Molecular Orbital Description of the O−O Bond Cleavage. Examination of the electronic structure changes along the reaction coordinate provides detailed insight into the orbital contributions to the O−O bond-cleavage reaction mechanism.

First, the spin density changes at the Cu centers in PI+e and PI+e+H upon elongation of the O^1-O^2 bonds are shown in Figure 8. The spin density at the $T3_B$ center remains constant throughout the reaction coordinate, indicating that this center remains fully oxidized. Alternatively, the magnitudes of the spin densities at the T2 and $T3_A$ centers gradually increase upon elongation of the O^1-O^2 bond, demonstrating that the reduced T2 and $T3_A$ centers gradually donate electrons in the reductive cleavage of the peroxide. Notably, the T2 and $T3_A$ spin densities increase symmetrically with opposite signs, reaching ~30−50% of their full values at NI, where these Cu centers are fully oxidized. This implies that the O−O bond cleavage is a simultaneous two-electron process.

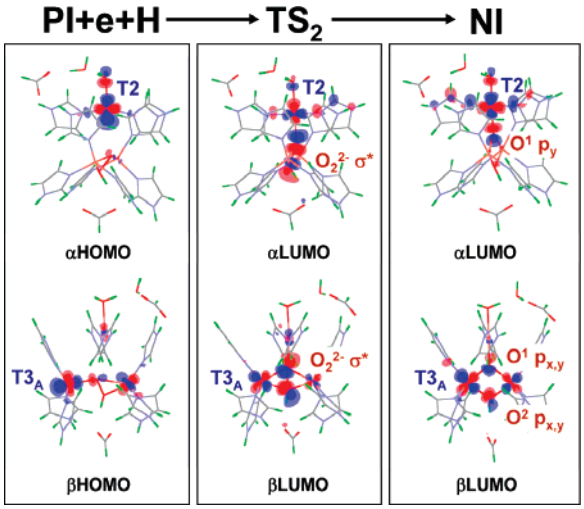

Figure 9. Correlation of MOs involved in electron transfer during the PI+e+H → TS_2 → NI process. In PI+e+H, only the $T3_B$ center is oxidized, and the α- and β-HOMOs are derived from the highest-energy d-electrons of T2 and $T3_A$ Cu centers. In TS_2, both the T2 $d_{x^2-y^2}$-based α-HOMO and $T3_A$ $d_{x^2-y^2}$-based β-HOMO form good overlap and mixing with the peroxide LUMO (O_2^{2-} σ^*) that promotes facile simultaneous two-electron transfer from the donor T2 and $T3_A$ Cu's to the acceptor peroxide for the O−O bond cleavage. In the final NI stage, the T2 and $T3_A$ Cu centers are fully oxidized and both O atoms fully reduced to μ_3-oxo (O^1) and μ-OH (O^2) bridging ligands. The same type of MO correlation can be made for the PI+e → TS_1 → NI process.

The MOs that are involved in the two-electron O−O bond-cleavage process in PI+e+H → TS_2 → NI are shown in Figure 9 (a similar description can be applied to the PI+e → TS_1 → NI process). According to the frontier molecular orbital (FMO) theory, the reaction is activated by good overlap between the HOMO of the donor (i.e., the reduced T2 and $T3_A$ Cu's) and the LUMO of the acceptor (i.e., the peroxide σ^*). At the start of the process, the two electrons of the donor T2 and $T3_A$ occupy the α- and β-HOMOs of PI+e+H (Figure 9, left), while the unoccupied O_2^{2-} σ^* is at high energy. As the O−O bond is elongated, the unoccupied O_2^{2-} σ^* decreases in energy and starts mixing with both the donor T2 $d_{x^2-y^2}$ and $T3_A$ $d_{x^2-y^2}$ HOMOs (Figure 9, middle). The strong orbital mixing at the transition state represents the efficiency of electron transfer from the donor T2 and $T3_A$ HOMOs to the acceptor peroxide LUMO, which is consistent with the low-energy barrier.

After the transition state, the electrons are fully transferred from the T2 and $T3_A$ Cu centers to both O atoms of the peroxide (i.e., fully oxidizing T2 and $T3_A$ and fully reducing O_2), completing the O−O bond cleavage (Figure 9, right). As described previously, the two O atoms become the μ_3-oxo and T3 μ-OH^- bridging ligands in NI that contribute significantly in stabilizing NI structure, providing the thermodynamic driving force for the four-electron reduction of O_2 in the MCOs.[25,27,28] It is worth mentioning that, while it is necessary to impose $|T2T3_AT3_B\rangle = |\beta\alpha\alpha\rangle$ spin configuration to generate the transient-state structures relevant to the PI+e/PI+e+H → NI process (vide supra), three broken-symmetry states $|\alpha\alpha\beta\rangle$, $|\alpha\beta\alpha\rangle$, and $|\beta\alpha\alpha\rangle$ equally contribute to the ground state of NI. This is due to the favorable super-exchange interactions among all three Cu centers via the μ_3-oxo and T3 μ-OH^- bridging ligands upon oxidation of the T2 and $T3_A$ centers (the second T3 μ-OH^- bridging ligand is found necessary to keep the three exchange coupling constants similar in NI, due to the difference

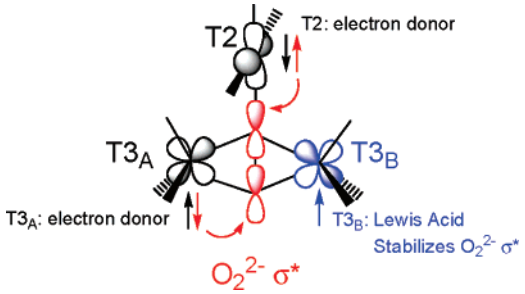

Figure 10. Orbital interactions in the O−O bond cleavage process.

in ligand environments between T2 and T3 sites[28]). Importantly, the interaction of the three broken-symmetry states results in the spin-frustrated ground state of NI. The unique properties of the ground state of NI are evidenced by features in its EPR and MCD spectra, where a low *g*-value <2.0 and a low-lying doublet excited state at ~150 cm^{-1} have been observed that are not possible for typical Cu(II) complexes.[18]

4. Discussion

Despite the strong experimental evidence that PI is the precursor for NI in the reaction mechanism of the MCOs, the geometric and electronic structure of PI has been elusive. It has been considered that the two-electron transfer to O_2 in the formation of PI occurs from the two T3 Cu's, in analogy to O_2-binding reactions in the other binuclear Cu sites in biology (Hc and Tyr). However, the T3 sites of MCO and Hc/Tyr are intrinsically different.[38−40,53,54,61] In particular, the T3 site in the T2-depleted form of tree Lc has been shown to lack any O_2 reactivity.[52−54] Interestingly, although the His ligand conformations are different in the T3 sites of MCOs and Hc/Tyr, our calculations on PI without D_{94} resulted in the side-on-bridged geometry that is very similar to those of the oxy-Hc and oxy-Tyr (Figure 2a). This suggests that the description of the trinuclear Cu cluster site must include the additional effects of the second-coordination sphere residues, in particular, D_{94}.

Inclusion of the D_{94} residue in our models allows us to obtain the spectroscopically relevant μ_3-1,1,2-bridged PI structure. Recent studies with Fet3p mutants have implicated the important role of the D_{94} residue,[23,31,34,35] where mutation of this residue to the uncharged Ala or Asn residue results in a complete loss of O_2 reactivity while its mutation into the negatively charged Glu retains the O_2 reactivity.[35,37] This suggests that the negative charge at the D_{94} position must induce a unique charge distribution in the trinuclear Cu cluster site that is necessary to stabilize the PI structure. Our calculations show that the inclusion of the negatively charged D_{94} results in the oxidation of the T2 and $T3_B$ centers with the $T3_A$ center reduced. Importantly, the μ_3-1,1,2-bridged geometry of PI would be closely related to the role of the trinuclear Cu cluster active site in biology, which is to irreversibly bind O_2 and activate it for the second two-electron step in the four-electron reduction of O_2 to H_2O. This is in contrast to the role of oxy-Hc with its side-on-bridged geometry, which is to reversibly bind and release O_2.

Evaluation of the PI+e → NI process using the 2D-PES (Figure 7) has provided insight into the rapid O−O bond-cleavage process in the MCOs. First, the reaction would be

(61) Hazes, B.; Magnus, K. A.; Bonaventura, C.; Bonaventura, J.; Dauter, Z.; Kalk, K. H.; Hol, W. G. J. *Protein Sci.* **1993**, *2*, 597−619.

driven by the large thermodynamic driving force ($\Delta E = -51$ kcal/mol, NI relative to PI+e) derived from the stable NI structure (relative to PI+e). The large exothermicity promotes the low-energy barrier of the O−O bond-cleavage process, which was calculated to be ~5−6 kcal/mol, consistent with the experimental value of 3−5 kcal/mol. Moreover, the spin density changes along the two possible reaction paths found in the 2D-PES (Figure 8) indicate that the two-electron reduction of the peroxide in the O−O bond cleavage proceeds via a simultaneous two-electron process and not two, sequential one-electron steps. This is consistent with the fact that the driving force of one-electron transfer from the T2/T3 Cu's ($E^0 \approx 0.4$ V) to peroxide is low ($E^0 = +0.38$ V vs NHE for $H_2O_2 + H^+ + e^- \rightarrow \bullet OH + H_2O$ at pH 7.0) whereas that of two-electron transfer is high ($E^0 = +1.35$ V vs NHE for $H_2O_2 + 2H^+ + 2e^- \rightarrow 2H_2O$ at pH 7.0).[62] Notably, this provides complementary evidence in support of the experimental results that NI is not a three-electron-reduced oxygen intermediate as previously proposed but rather a four-electron product.[19,20,63−65]

The efficient O−O bond cleavage is also closely related to the triangular topology of the trinuclear Cu cluster. In the transition states (i.e., TS_1 and TS_2), the triangular arrangement of the Cu centers allows the acceptor O_2^{2-} σ^* MO to have strong σ-overlaps with both the donor T2 and $T3_A$ $d_{x^2-y^2}$ MOs (Figure 10) that promote facile two-electron donation and the low activation barrier. Furthermore, it is worth mentioning that, while the $T3_B$ center does not contribute directly in electron donation to PI, this positively charged oxidized Cu^{II} center would contribute in lowering the O_2^{2-} σ^* energy. The orbital mixing of the half-occupied $d_{x^2-y^2}$ orbital of the oxidized $T3_B$ center and the unoccupied O_2^{2-} σ^* via good σ-overlap is, again, promoted in the trigonal arrangement of the trinuclear Cu cluster (Figure 10). Consequently, O_2^{2-} σ^* character would be present in the lower-energy half-occupied $T3_B$ MO, which would energetically enhance the donor−acceptor interaction with the reduced T2 and $T3_A$ MOs. This role of $T3_B$ is of particular importance for the proton-unassisted process.

Thus, the O−O bond cleavage in MCOs does not intrinsically require the assistance of the proton, allowing the reaction to proceed efficiently at high as well as at low pH. In cytochrome *c* oxidase (CcO), on the other hand, it has been proposed that protonation of the peroxide by the Tyr residue near the binuclear heme-Cu_B active site is necessary prior to the O−O bond cleavage to achieve a low-energy barrier to produce the ferryl-oxo-level P_M intermediate.[66−68] The distinction between the heme-Cu_B site of CcO and the trinuclear Cu cluster site in MCO lies in the fact that in the MCOs there are three Cu centers present that are capable of serving both as the source of electrons (the reduced Cu^I) and as Lewis acids (the oxidized Cu^{II}) in place of a H^+ for the efficient four-electron reduction of O_2. In the binuclear heme-Cu_B site of CcO, a counterpart of the oxidized $T3_B$ center is not available, and thus, O−O bond cleavage would require a proton to assist lowering the O_2^{2-} σ^* orbital for favorable donor−acceptor FMO interactions.

In summary we have shown that O_2 binds in a fundamentally different way in the trinuclear Cu cluster relative to the T3 sites in Hc/Tyr in that it bridges the T2 and T3 Cu's due to the presence of D_{94} near the T2 site. This likely stabilizes the peroxide-bound structure against loss of O_2. The trinuclear Cu cluster further promotes cleavage of the O−O bond by having FMOs specifically oriented for overlap with σ^* LUMO of peroxide and by stabilizing the product of peroxide reduction through bridging at the trinuclear site in NI.

Acknowledgment. We thank A. J. Augustine for helpful discussion regarding the kinetics of PI formation and decay. This research was supported by NIH Grants DK31450. J.Y. gratefully acknowledges a Franklin Veatch Memorial Fellowship.

Supporting Information Available: Complete ref 42, the geometric parameters and spin densities of different PI structures calculated, the calculated results of the 28 points used in generating the 2D-PES, and the Cartesian coordinates of PI (with D_{94}), PI+e, PI+e+H, TS_1, TS_2, and NI. This material is available free of charge via the Internet at http://pubs.acs.org.

JA073947A

(62) Sawyer, D. T. *Oxygen Chemistry*; Oxford University Press: New York, 1991.
(63) Aasa, R.; Brändén, R.; Deinum, J.; Malmström, B. G.; Reinhammar, B.; Vänngård, T. *Biochem. Biophys. Res. Commun.* **1976**, *70*, 1204−1209.
(64) Andréasson, L. E.; Brändén, R.; Reinhammar, B. *Biochim. Biophys. Acta* **1976**, *438*, 370−379.
(65) Huang, H.-W.; Zoppellaro, G.; Sakurai, T. *J. Biol. Chem.* **1999**, *274*, 32718−32724.
(66) Blomberg, M. R. A.; Siegbahn, P. E. M. *Biochim. Biophys. Acta* **2006**, *1757*, 969−980.
(67) Blomberg, M. R. A.; Siegbahn, P. E. M. *J. Comput. Chem.* **2006**, *27*, 1373−1384.
(68) Blomberg, M. R. A.; Siegbahn, P. E. M.; Wikstrom, M. *Inorg. Chem.* **2003**, *42*, 5231−5243.